Am J Physiol Gastrointest Liver Physiol 324: G378–G388, 2023.
First published February 28, 2023; doi:10.1152/ajpgi.00157.2022

american physiological society

AMERICAN JOURNAL OF PHYSIOLOGY
GASTROINTESTINAL AND LIVER PHYSIOLOGY

RESEARCH ARTICLE

Hepatoprotective effects of the long-acting fibroblast growth factor 21 analog PF-05231023 in the GAN diet-induced obese and biopsy-confirmed mouse model of nonalcoholic steatohepatitis

Malte Hasle Nielsen,[1,2] Matthew P. Gillum,[2] Niels Vrang,[1] Jacob Jelsing,[1] Henrik H. Hansen,[1] Michael Feigh,[1] and Denise Oró[1]

[1]*Gubra, Horsholm, Denmark and* [2]*Novo Nordisk Foundation Center for Basic Metabolic Research, University of Copenhagen, Copenhagen, Denmark*

Abstract

Fibroblast growth factor 21 (FGF21) plays a key role in hepatic lipid metabolism and long-acting FGF21 analogs have emerged as promising drug candidates for the treatment of nonalcoholic steatohepatitis (NASH). It remains to characterize this drug class in translational animal models that recapitulate the etiology and hallmarks of human disease. To this end, we evaluated the long-acting FGF21 analog PF-05231023 in the GAN (Gubra Amylin NASH) diet-induced obese (DIO) and biopsy-confirmed mouse model of NASH. Male C57BL/6J mice were fed the GAN diet high in fat, fructose, and cholesterol for 34 wk before the start of the study. GAN DIO-NASH mice with biopsy-confirmed NAFLD Activity Score (NAS $\geq$5) and fibrosis (stage $\geq$F1) were biweekly administered with PF-05231023 (10 mg/kg sc) or vehicle (sc) for 12 wk. Vehicle-dosed chow-fed C57BL/6J mice served as healthy controls. Pre-to-post liver biopsy histopathological scoring was performed for within-subject evaluation of NAFLD Activity Score (NAS) and fibrosis stage. Terminal endpoints included quantitative liver histology and transcriptome signatures as well as blood and liver biochemistry. PF-05231023 significantly reduced body weight, hepatomegaly, plasma transaminases, and plasma/liver lipids in GAN DIO-NASH mice. Notably, PF-05231023 reduced both NAS ($\geq$2-point improvement) and fibrosis stage (1-point improvement). Improvements in NASH and fibrosis severity were supported by reduced quantitative histological markers of steatosis, inflammation, and fibrogenesis as well as improvements in disease-associated liver transcriptome signatures. In conclusion, PF-05231023 reduces NASH and fibrosis severity in a translational biopsy-confirmed mouse model of NASH, supporting development of FGF21 analogs for the treatment of NASH.

NEW & NOTEWORTHY It is unclear if long-acting FGF21 analogs have antifibrotic efficacy in NASH. We therefore profiled the clinically relevant FGF21 analog PF-05231023 in a translational diet-induced obese and biopsy-confirmed mouse model of NASH. We found PF-05231023 to exert hepatoprotective effects as indicated by notable improvements in plasma markers and histological hallmarks of NASH, including improved fibrosis stage. Collectively, the present study supports the continued exploration of long-acting FGF21 analogs for the treatment of NASH and other fibrotic diseases.

fibroblast growth factor 21; fibrosis; liver biopsy; nonalcoholic steatohepatitis; translational model

INTRODUCTION

Nonalcoholic fatty liver disease (NAFLD) is the most common cause of chronic liver disease in the Western world and a major risk factor for cirrhosis and hepatocellular carcinoma (1). The prevalence of NAFLD is rising in parallel with the global increase in obesity and type 2 diabetes, which are major risk factors for the onset and progression of the disease. The most severe form of NAFLD, nonalcoholic steatohepatitis (NASH), is characterized by steatosis, lobular inflammation, and hepatocyte injury (ballooning) with or without fibrosis (2). Currently, there exist no FDA-approved medications for NASH, making liver transplantation the only available curative treatment option for cirrhosis. The unmet need for effective treatments has prompted intense target discovery research, and multiple drug development programs are at various stages of clinical development (3).

Fibroblast growth factor 21 (FGF21) is a peptide hormone primarily expressed and secreted from the liver (4). The biological actions of FGF21 are mainly mediated through binding to the FGF receptor 1 (FGFR1), and to a lesser extent FGFR2, FGFR3, and FGFR4, in conjunction with the obligate coreceptor β-klotho (KLB) (4). Accumulating evidence points to a wide range of metabolic functions of FGF21 that vary by species. These include regulation of energy balance and glucose and lipid homeostasis as well as the mediation of interorgan metabolic cross talk, conferring beneficial actions in

Correspondence: M. H. Nielsen (mni@gubra.dk).
Submitted 23 June 2022 / Revised 17 January 2023 / Accepted 20 February 2023

obesity, type 2 diabetes, and related comorbidities, including NAFLD (5, 6).

The metabolic effects of FGF21 are mediated at both the peripheral and central levels. Peripheral actions include targeting adipose tissue to increase glucose uptake (7, 8), lipid disposal (9), and adiponectin secretion (10). At the central level, rodent studies have pointed to FGF21-induced adipose tissue browning and thermogenesis by stimulation of paraventricular hypothalamic sympathetic activity (11). FGF21 has also consistently been reported to modulate food intake, sugar preference, and alcohol consumption by targeting KLB-expressing neurons in the basolateral amygdala and suppressing mesolimbic dopaminergic neurotransmission (12, 13). The role of FGF21 in regulating liver metabolism is complex and incompletely understood due to interconnected FGF21-producing target tissues and organs as well as the endocrine, paracrine, and autocrine functions of FGF21 (4). The hepatic effects of FGF21 are likely afforded by a combination of intrahepatic and extrahepatic mechanisms involving direct hepatocyte metabolic actions, stimulation of adipocyte-secreted adiponectin, and brain-liver cross talk to promote body weight loss with concurrent improvements in glycemic control and lipid profile (4, 5).

The clinical use of native FGF21 is limited due to its short circulating half-life (30 min to 2 h) (14). To circumvent this limitation, long-acting FGF21 analogs have been developed and evaluated in clinical trials for the treatment of metabolic diseases including obesity, type 2 diabetes, dyslipidemia, and NAFLD. These studies have consistently reported reductions in levels of triglycerides (TGs) and total cholesterol (TC) and increased levels of high-density lipoprotein cholesterol (HDL-C) and adiponectin (14–18). Moreover, improvement of liver fibrosis and stiffness biomarkers have been shown in response to treatment with FGF21 analogs Pegbelfermin and AKR-001 in human NASH and patients with type 2 diabetes (18, 19). To improve pharmacokinetics of FGF21, several approaches such as Fc fusion (19), PEGylation (20), introduction of disulfide bonds (21), and antibody conjugation (22) have been employed. For example, the FGF21 analog PF-05231023 has been engineered for extended half-life and bioavailability by conjugating two recombinant human FGF21 proteins to the Fab region of human immunoglobulin G (22).

In genetic and diet-induced mouse models of obesity, the administration of FGF21 analogs has been demonstrated to drive robust reductions in body weight and adiposity while also improving glycemic control, insulin sensitivity, and levels of triglycerides and cholesterol (14). In the context of NAFLD, administration of FGF21 analogs consistently reduce hepatic steatosis and inflammation in a diverse set of diet-induced, genetically modified, or chemically induced rodent models of NASH (14). In support of therapeutic effects of FGF21 in NAFLD, FGF21 deficiency worsens the NASH phenotype in mice (23, 24).

To date, therapeutic benefits of FGF21 analogs have only been reported in nonphysiological models of NASH such as genetically and chemically induced mouse models (25–28). Given the therapeutic potential of FGF21 analogs in NASH, it is important to characterize these analogs in a more clinically translational animal model. A novel high-caloric diet-induced obese and biopsy-confirmed mouse model of progressive NASH and fibrosis has recently been profiled extensively with respect to human translatability. Accordingly, the GAN (Gubra Amylin NASH) diet-induced obese (DIO) and biopsy-confirmed mouse model of NASH recapitulates the various histological stages of NASH with progressive fibrosis (29–38). The GAN diet closely resembles the AMLN diet (29), which has been extensively validated for inducing a clinical translational metabolic and histopathological phenotype in mice (39–42). Correspondingly, GAN DIO-NASH mice demonstrate a consistent obese and dysmetabolic profile characterized by impaired glucose tolerance, hyperinsulinemia, increased HOMA-IR index (a valid measure of systemic insulin resistance) as well as hypercholesterolemia and hyperleptinemia (30, 31). Normal baseline glucose levels in the context of hyperinsulinemia in GAN DIO-NASH mice suggest pancreatic β-cell compensation (30) and an insulin-resistant phenotype (30, 31). Importantly, the GAN DIO-NASH model faithfully reproduces histological efficacy profiles of compounds in advanced clinical development for NASH (29–31, 43) thus representing an attractive model for exploring FGF21 pharmacological intervention. PF-05231023 has been reported to exert both body weight-dependent and -independent metabolic effects in patients with diabetes and obesity (44, 45). Although these data have been corroborated in mouse and nonhuman primate studies (46, 47), it is not known if the metabolic benefits of PF-05231023 could translate into beneficial effects in NASH. The present study therefore aimed to profile PF-05231023 in the GAN DIO-NASH mouse.

METHODS

Ethics

All animal experiments were approved by The Danish Animal Experiments Inspectorate (License No. 2017-15-0201–01378). Animal experiments were conducted in agreement with internal Gubra bioethical guidelines that are fully compliant with internationally accepted principles for the care and use of laboratory animals.

Animals

C57BL/6J mice (5 wk old) were purchased from Janvier Labs (Le Genest, Saint Isle, France) and housed in a controlled environment (12 h light/dark cycle, lights on at 3:00 AM, 21 ± 2°C, humidity 50 ± 10%). Each animal was implanted with a subcutaneous microchip (PetID Microchip, E-vet, Haderslev, Denmark) for identification. Animals had ad libitum access to tap drinking water and chow (3.22 kcal/g, Altromin 1324, Brogaarden, Hoersholm, Denmark) or Gubra Amylin NASH diet [GAN diet, 4.49 kcal/g, 40 kcal-% fat (of these 46% saturated fatty acids by weight), 22% fructose, 10% sucrose, 2% cholesterol; D09100310, Research Diets] (29) for 34 wk before treatment start and maintained on the diet throughout the 12-wk study period. Mice were euthanized by cardiac puncture under isoflurane anesthesia (Vetflurane, Virbac, Kolding, Denmark).

Baseline Liver Biopsy

Mice were subjected to a liver biopsy, as previously described in detail (40). In brief, animals were anesthetized with isoflurane, and a midline abdominal incision was performed exposing the left lateral lobe. A cone-shaped biopsy

of ~50 mg liver tissue was collected, cut surfaces were electrocoagulated using an electrosurgical unit (ERBE VIO 100 C, ERBE, Marietta, GA), the liver was returned to the abdominal cavity, and the abdominal wall was sutured and the skin was stapled. Mice received 5 mg/kg carprofen (Norodyl, ScanVet, Fredensborg, Denmark) before surgery and on *day 1* and *2* postsurgery. Animals were single-housed after the operation and allowed to recover for 4 wk before the start of treatment.

Treatment Intervention

Study inclusion criteria for GAN DIO-NASH mice were biopsy-confirmed NAFLD Activity Score (NAS ≥5) and the presence of fibrosis (stage ≥F1), evaluated by standard clinical histopathological scoring criteria as outlined by Kleiner et al. (48). Subsequently, animals were randomized and stratified to treatment based on fibrosis proportionate percent area of picrosirius red (PSR) staining. GAN DIO-NASH mice were biweekly administered (SC) vehicle or the FGF21 analog PF-05231023 for 12 wk (n = 14/group). Chow-fed mice, serving as lean controls, received saline vehicle (Chow vehicle, subcutaneous) for 12 wk (n = 6). PF-05231023 was dissolved in phosphate-buffered saline. Vehicle and FGF21 were administered in a dosing volume of 5 mL/kg. Body weight was measured daily and 24 h food intake was measured once weekly during the treatment intervention period.

Plasma and Liver Biochemistry

Blood was collected from the tail vein on the morning of termination, kept on ice, and centrifuged (5 min, 4°C, 6,000 *g*) to give EDTA-stabilized plasma. Plasma alanine aminotransferase (ALT), aspartate aminotransferase (AST), triglycerides (TGs), total cholesterol (TC), and liver TG and TC were determined as described previously (41). For hydroxyproline (HP) determination, quick-frozen liver tissue (100 mg) was homogenized in 6 M HCl and hydrolyzed to degrade collagen. Hydroxyproline content was then measured in the supernatant using a colorimetric kit (Cat. No. QZBHYPRO5, Quickzyme Biosciences, Leiden, The Netherlands) according to the manufacturer's instructions.

Liver Histology

Baseline liver biopsy and terminal biopsy, both sampled from the left lateral lobe, were fixed overnight in 4% paraformaldehyde. Tissue was paraffin-embedded and sectioned at 3μm thickness. Liver biopsy sections were stained with hematoxylin-eosin (HE, Dako, Glostrup, Denmark), picrosirius red (PSR, Sigma Aldrich, Brondby, Denmark), anti-galectin-3 (Gal-3, Cat. No. 125402, BioLegend, San Diego, CA), anti-type I collagen (Col1a1, Cat. No. 1310-01, Southern Biotech, Birmingham, AL), or α-smooth muscle actin (α-SMA, Cat. No. Ab124964, Abcam, Cambridge, UK) according to standard protocols (40, 41). See Supplemental Table S1 (see https://doi.org/10.6084/m9.figshare.21424488.v1) for further details on the histological staining procedures. Histopathological scoring of steatosis, lobular inflammation, hepatocyte ballooning, and fibrosis staging was performed by Gubra Histopathological Objective Scoring Technique (GHOST) automated deep learning-based image analysis (31) using the NASH Clinical Research Network (CRN) scoring system (48). NAS and fibrosis stages were compared with baseline scores for within-subject evaluation of treatment efficacy. GHOST deep learning-based image analysis was further applied for histomorphometric assessment of histopathological scoring-associated variables, including fraction of lipid-laden hepatocytes (%), number of inflammatory foci (foci/mm^2), and percent proportionate area fibrosis. In addition, quantitative histology was performed using a digital imaging software (Visiomorph, Visiopharm, Hørsholm, Denmark) for the determination of liver fat (HE-staining), fibrosis (PSR, Col1a1), inflammation (galectin-3), and activated stellate cells (α-SMA) expressed relative (%) to total sectional area. To account for changes in liver mass resulting from treatment intervention, the percent area of positive staining was multiplied with the corresponding total liver weight as an estimate of total liver marker content (mg); a procedure previously validated to be representative of whole liver histological changes in obese mouse models of NASH (49).

RNA Sequencing

RNA was extracted from snap-frozen terminal liver samples (~20 mg fresh tissue) and liver transcriptome analysis was performed by RNA sequencing analysis, as previously described in detail (30, 31). RNA sequence libraries were prepared using NeoPrep (Illumina, San Diego, CA) and the Illumina TruSeq stranded mRNA Library kit for NeoPrep (Illumina, San Diego, CA) and sequenced using the NextSeq 500 (Illumina, San Diego, CA) with NSQ 500 hi-Output KT v2 (75 CYS, Illumina, San Diego, CA). The reads were aligned to the GRCm38 v84 Ensembl *Mus musculus* genome by applying the STAR v.2.5.2a with default parameters. The lower detection limit for gene expression was set at 0.1 RPKM. Differential gene expression analysis was performed using the DESeq2 *R*-package, and gene set analysis using the PIANO version 1.18.1 *R*-package and using the Stouffer method. The Reactome pathway database (50) was used for gene annotation in the gene set analysis. The Benjamini–Hochberg method (5% False Discovery Rate, FDR < 0.05) was used for multiple testing correction of *P* values.

Statistics

Data are presented as means ± SE. Except from gene expression data, Dunnett's test one-factor linear model with interaction was applied, with initial comparison of vehicle control groups (DIO-NASH vs. Chow), followed by analysis of PF-05231023 treatment response (PF-05231023 DIO-NASH vs. Vehicle DIO-NASH). A P value of <0.05 was considered statistically significant.

RESULTS

PF-05231023 Improves Body Weight, Hepatomegaly, and Biochemical Markers

PF-05231023 significantly decreased body weight (−8%, $P < 0.001$ compared with baseline) after 12 wk of treatment in DIO-NASH mice (Fig. 1*A*). In comparison, vehicle controls gained 4% (chow) and 10% (DIO-NASH) body weight over the study period. Compared with vehicle-dosed DIO-NASH mice, PF-05231023 significantly increased caloric intake over the treatment period (Fig. 1*B*). Hepatomegaly was

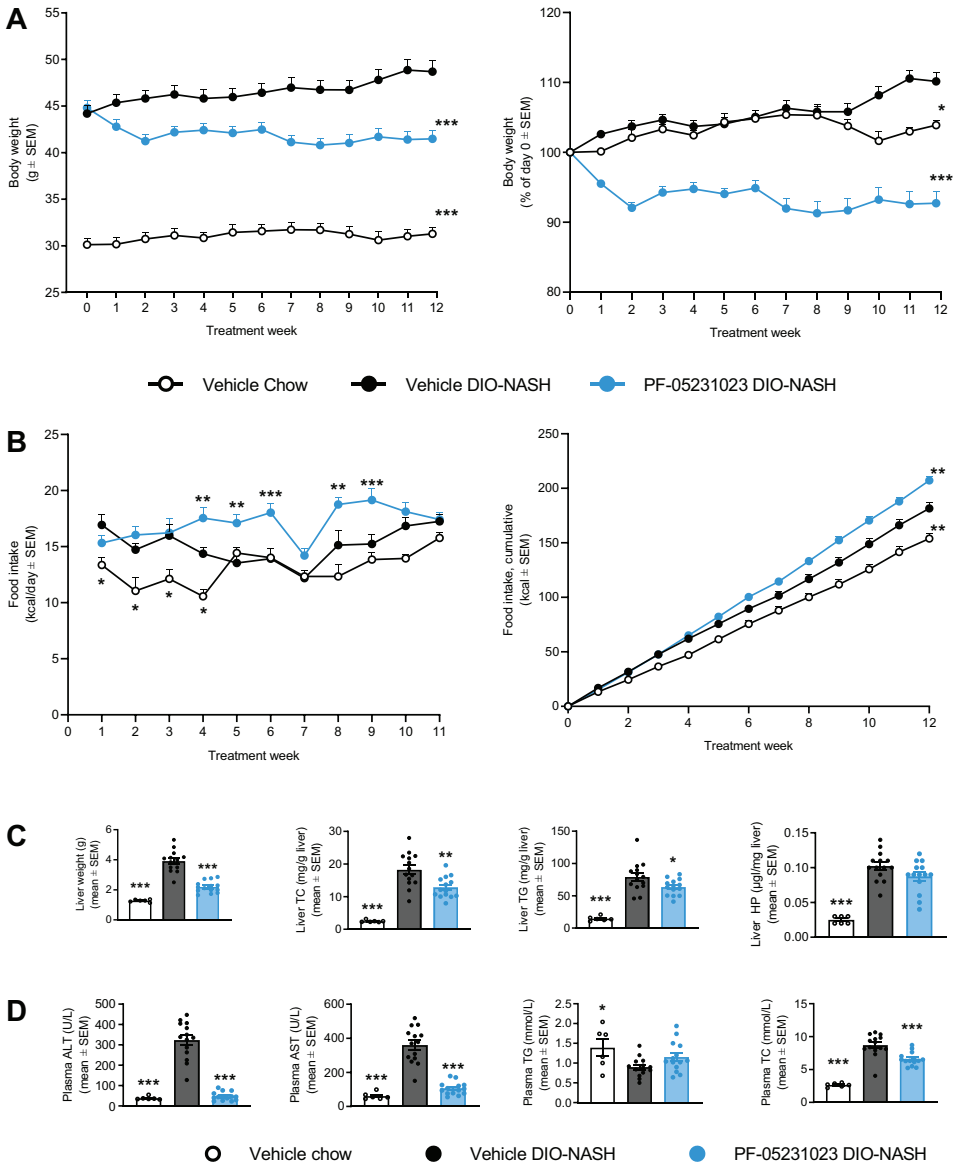

Figure 1. Effect of 12 wk of treatment with vehicle or PF-05231023 on metabolic parameters, food intake, and biochemical parameters in GAN DIO-NASH mice. *A*: absolute body weight and percent change relative to baseline (*day 0*). *B*: daily and cumulative food intake. *C*: liver weight and liver biochemistry for total cholesterol (TC), triglycerides (TG), and hydroxyproline (HP). *D*: plasma biochemistry for alanine aminotransferase (ALT), aspartate aminotransferase (AST), triglycerides (TG), and total cholesterol (TC). n = 6–14 mice/group, *$P < 0.05$, **$P < 0.01$, ***$P < 0.001$ (Dunnett's test one-factor linear model). DIO, diet-induced obese; GAN, Gubra Amylin NASH; NASH, nonalcoholic steatohepatitis.

significantly improved in PF-05231023-treated animals displaying a 44% reduction ($P < 0.001$) in liver weight compared with vehicle-dosed DIO-NASH controls (Fig. 1*C*). PF-05231023 significantly reduced liver TC and TG, whereas liver HP levels were unaffected (Fig. 1*C*). PF-05231023 also significantly lowered ALT, AST, and TC plasma levels (Fig. 1*D*).

PF-05231023 Improves Liver Histopathological Hallmarks of NASH

Compared with baseline, NAS was consistently reduced after PF-05231023 treatment, with 13 of 14 animals (93%) demonstrating ≥1-point improvement, driven by reductions in steatosis scores ($P < 0.001$) and lobular inflammation scores ($P < 0.05$; Fig. 2, *A* and *B*). Eight of 14 animals (57%) showed ≥2 point improvement in NAS (Fig. 2*A*). See Fig. 2*C* for individual pre- to post-changes in histopathological scores. PF-05231023 induced a significant 1-point improvement of fibrosis stage in 4 of 14 mice ($P < 0.05$ vs. Vehicle DIO-NASH, Fig. 2, *A* and *C*). In support of improved hallmarks of NASH, PF-05231023 significantly reduced quantitative markers of steatosis (% hepatocytes with lipid droplets, $P < 0.001$; % area of lipids, $P < 0.001$; Fig. 3, *A* and *B*) and inflammation (number of inflammatory foci, $P < 0.05$; % area of galectin-3, $P < 0.001$; Figs. 3*C* and 4*A*). Although having no effect on quantitative markers of fibrosis (% area of PSR and Col1a1, Figs. 3*D* and 4*B*), PF-05231023 significantly reduced total liver PSR ($P < 0.01$) and Col1a1 ($P < 0.01$) content (Figs. 3*E* and 4*E*) as a result of decreased hepatomegaly. Also, PF-05231023 significantly reduced %-area of α-SMA ($P < 0.001$; Fig. 4*C*), a marker of hepatic stellate cell (HSC) activation.

PF-05231023 Improves Gene Expression Signatures Associated with NASH

A principal component analysis (PCA) of the 500 most variable genes showed clear group-wise clustering of regulated genes. Notably, global gene expression signatures in PF-05231023-treated DIO-NASH mice were clearly separated

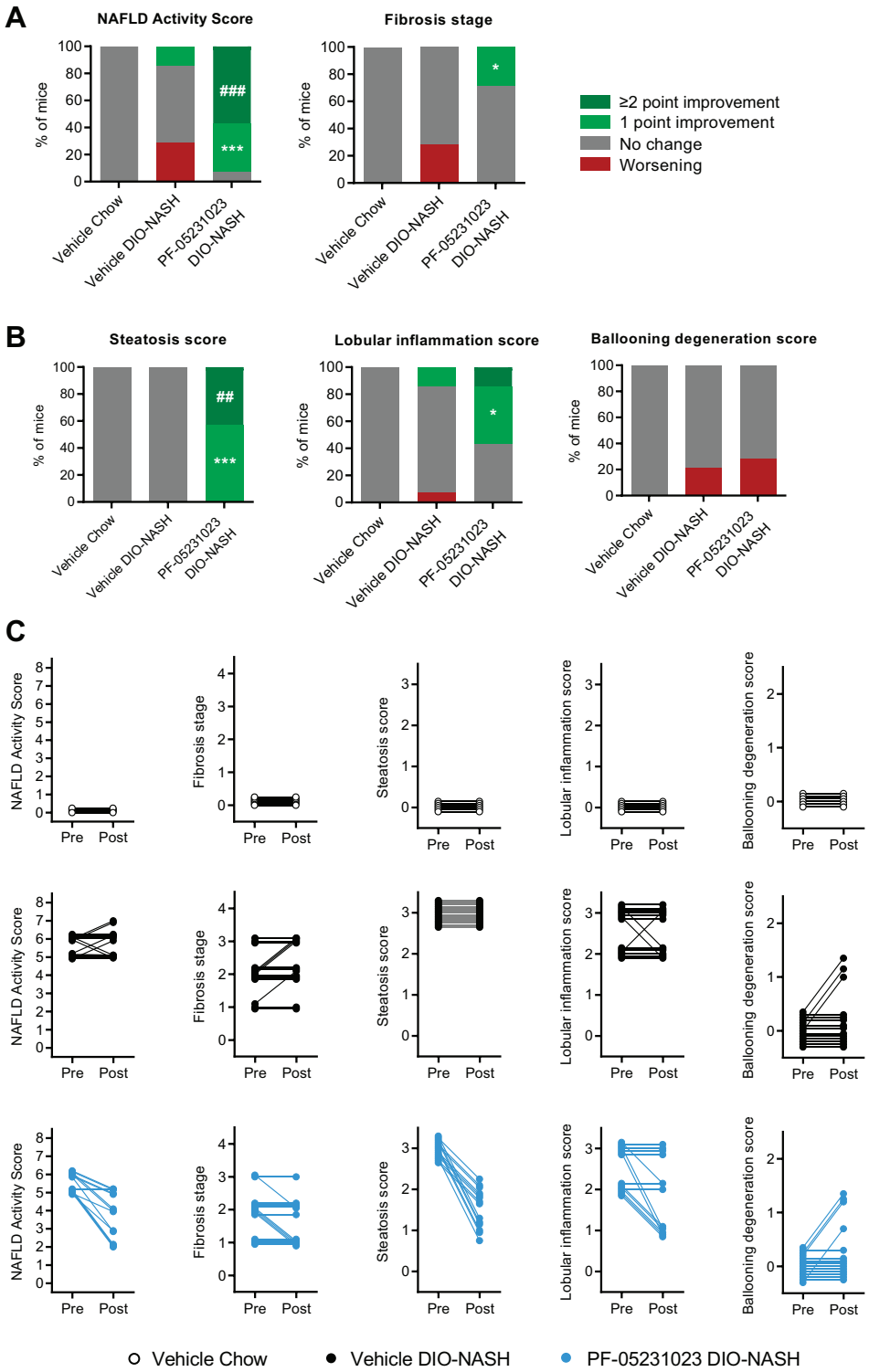

Figure 2. PF-05231023 improves liver histopathological NAFLD Activity Score and fibrosis stage in GAN DIO-NASH mice. Histopathological scores were determined by Gubra Histopathological Objective Scoring Technique (GHOST) deep learning-based image analysis. Summary of changes in pre-to-post histopathological scores for (*A*) NAFLD Activity Score (NAS) and fibrosis stage (*B*) and steatosis, lobular inflammation and ballooning degeneration score. Vehicle-dosed chow-fed mice served as normal controls. n = 6–14 mice/group, $^{*}P < 0.05$, $^{***}P < 0.001$ for $\geq$1 point improvement, $^{\#\#}P < 0.01$, $^{\#\#\#}P < 0.001$ for $\geq$2 point improvement (one-sided Fisher's exact test with Bonferroni correction). *C*: comparison of individual pre-to-post liver biopsy histopathological scores for NAS, fibrosis stage, steatosis score, lobular inflammation score, hepatocyte ballooning degeneration score in GAN DIO-NASH mice administered vehicle or PF-05231023 for 12 wk. DIO, diet-induced obese; GAN, Gubra Amylin NASH; NASH, nonalcoholic steatohepatitis.

from vehicle-dosed controls demonstrating a large number (n = 3,774) of differentially expressed genes (DEGs) (Fig. 5, *A* and *B*). Of these, 2078 DEGs were shared by the chow control group. Although *Fgf21* gene expression was upregulated in vehicle-dosed DIO-NASH, cognate receptors/coreceptors *Klb* and *Fgfr4* were downregulated (Fig. 5*C*). Treatment with PF-05231023 treatment decreased *Fgf21* expression and increased expression of *Klb*, *Fgfr2*, and *Fgfr4* compared with vehicle DIO-NASH. PF-05231023 treatment resulted in significant regulation of NASH-associated candidate genes compared with vehicle controls. These include upregulation of genes related to glucose metabolism (*Foxo1*, *Gys2*, *Insr*, *Irs1*, *Map2k2*, *Pck1*, and *Pygl*), bile acid metabolism (*Abcb11*, *Slc10a2*, *Slc27a5*, and *Slco1a4*), lipid metabolism (*Acaca*, *Acacb*, *Apoa1*, *Apoc2*, *Hmgcr*, *Hmgcs2*, *Ldlr*, *Lrp1*, *Ppard*, *Scarb1*, *Thrb*, and *Vldlr*) and ER stress (Ern1) (Fig. 5*D*). Concurrently, PF-05231023

AJP-Gastrointest Liver Physiol • doi:10.1152/ajpgi.00157.2022 • www.ajpgi.org

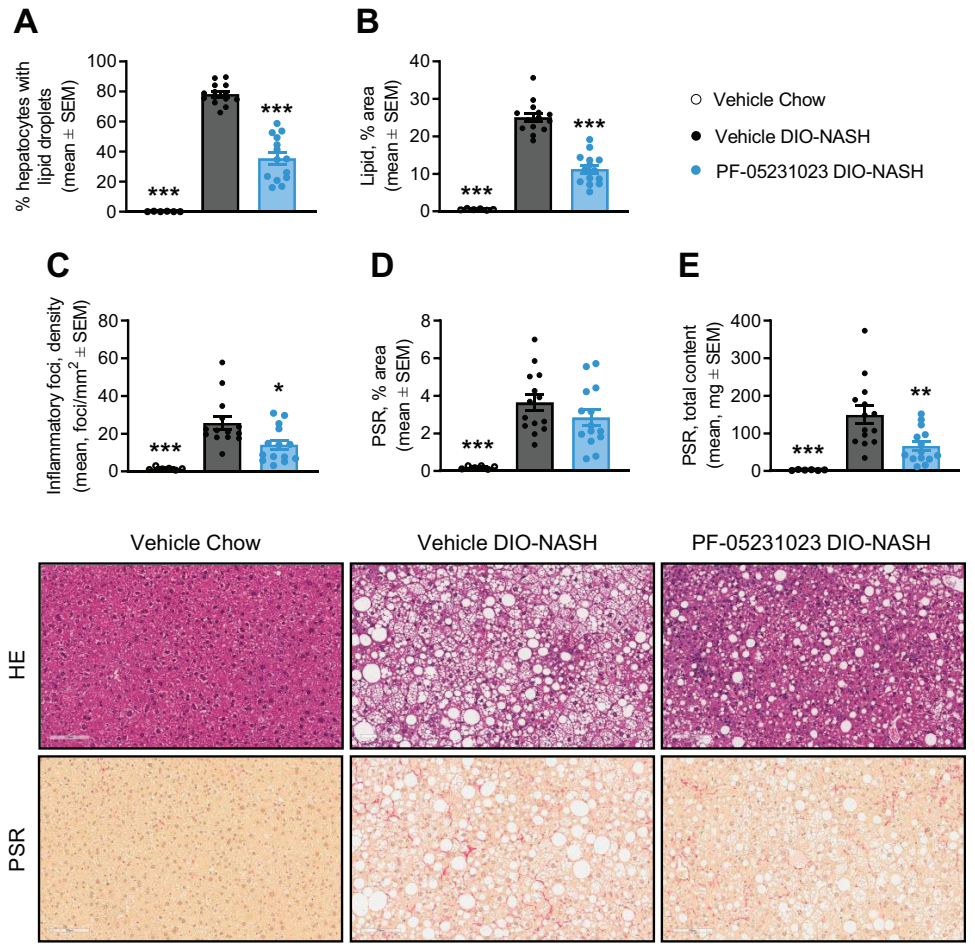

Figure 3. PF-05231023 improves quantitative histology of steatosis, inflammation, and fibrosis in GAN DIO-NASH mice. *A*: percent hepatocytes with lipid droplets. *B*: lipid percent area. *C*: inflammatory foci density. *D*: picrosirius red (PSR) percent area. *E*: PSR total count. n = 6–14 mice/group, $^{*}P < 0.05$, $^{**}P < 0.01$, $^{***}P < 0.001$ (Dunnett's test one- factor linear model). *Bottom* panels: representative HE and PSR photomicrographs used for GHOST evaluation. DIO, diet-induced obese; GAN, Gubra Amylin NASH; GHOST, Gubra Histopathological Objective Scoring Technique; NASH, nonalcoholic steatohepatitis; HE, hematoxylin-eosin; PSR, picrosirius red.

downregulated genes related to hepatocellular cell injury/death (*Aim2, Casp1, Nlrp3,* and *Ripk3*), inflammation (*Adgre1, Ccl2, Ccr1, Ccr2, Ccr5, Cd14, Cd68, Cd86, Cysltr1, Il1b, Lgals3, Tgfbr1, Tlr4*, and *Tnf*), and ECM remodeling (*Acta2, Col1a2, Col3a1, Col5a2, Ctsk, Efemp1, Fbln5, Loxl2, Mcam, Mmp24, Pdgfa, Serpinh1, Tgfb1, Timp1*, and *Vcan*).

DISCUSSION

To date, therapeutic efficacy of FGF21 analogs in NASH has been supported by preclinical studies in nonphysiological rodent models. This study is the first to demonstrate that a long-acting FGF21 analog improves NASH and fibrosis severity in a translational diet-induced obese mouse model of biopsy-confirmed NASH and fibrosis, suggesting clinical utility of FGF21 analogs in the management of fibrosing NASH.

The antisteatotic and anti-inflammatory effects of PF-05231023 are consistent with previous leptin-deficient obese mouse and nonhuman primate studies (46, 47) as well as in line with clinical studies in diabetic and obese human subjects (44, 45). Notably, the present study indicated that PF-05231023 promoted a 1-point significant improvement in fibrosis stage. Clinical trials on FGF21 analog treatment in patients with NASH remain few and with small sample sizes. For example, in a recent phase 2a clinical trial evaluating an FGF21 fusion protein, more than half of the subjects had a ≥1 improvement in fibrosis stage (17). The improvement of fibrosis stage shown by histopathological scoring in our study is supported by reduced α-SMA levels, a reliable marker for activation of HSCs, which are the principal collagen-producing cells in the liver (51). In contrast, quantitative assessment of fibrosis by proportionate area of PSR and Col1a1 staining showed no significant improvement, which could suggest that PF-05231023 changes the distribution of collagen fibers without altering overall collagen levels. Importantly, redistribution of collagen (toward a lower score) is associated with improved outcomes in NASH (52, 53).

Treatment with PF-05231023 in GAN DIO-NASH mice led to a significant body weight reduction which is consistent with previous reports on treatment with FGF21 analogs in diet-induced and genetic mouse models of obesity (14). As in the clinic, treatment interventions causing weight loss could per se have beneficial effects on liver biochemical and histological endpoints in GAN DIO-NASH mice. Accordingly, weight loss accompanied by improvements in liver parameters has previously been reported in GAN DIO-NASH mice on long-term treatment with various compounds in clinical development for NASH (31, 41). It should be noted that weight loss effects of PF-05231023 were contrasted by a modest, however significant, increase in food intake. Previous studies in rodent models of obesity have demonstrated unchanged or slightly increased food intake when expressed relative to body weight (14, 54, 55). Similar to our study in

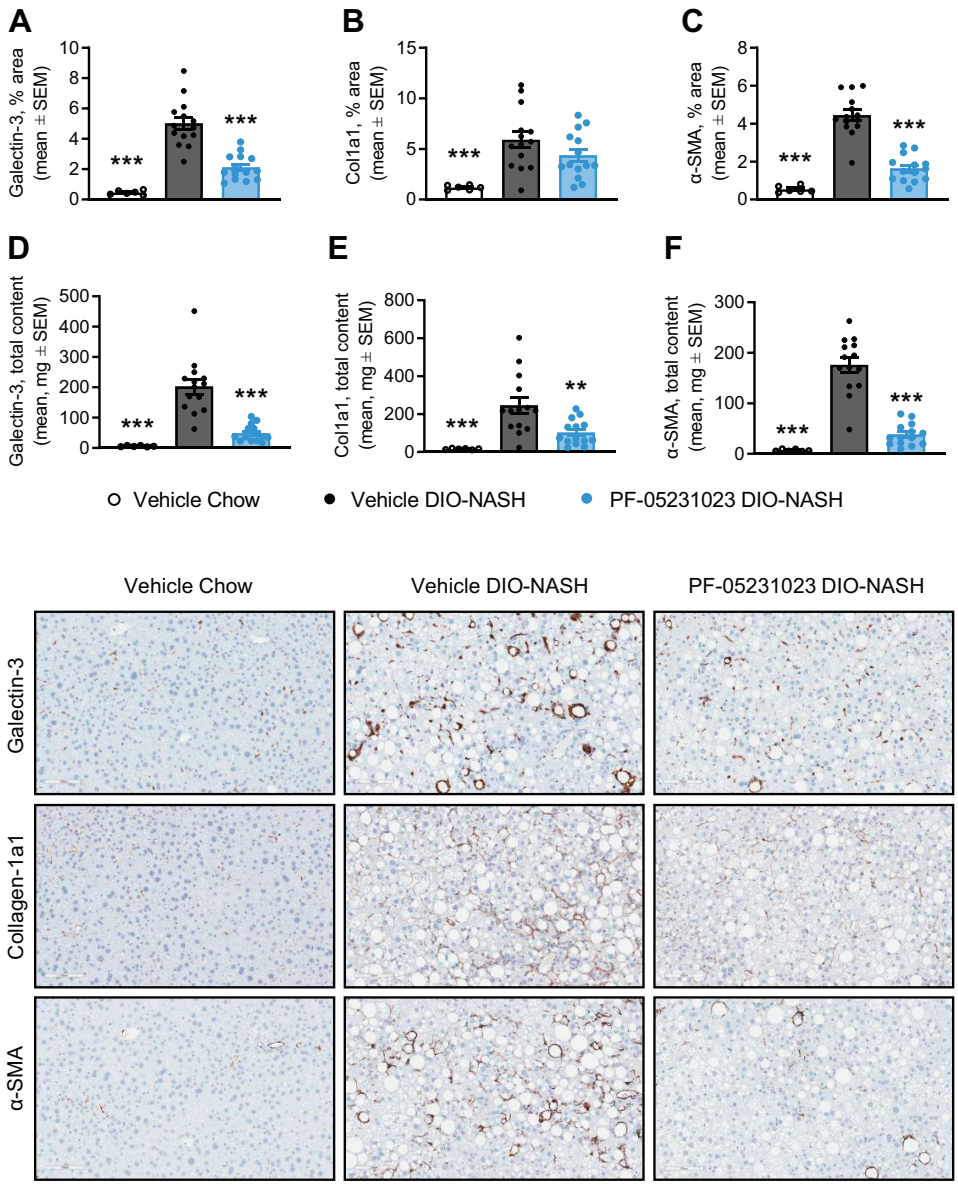

Figure 4. Improvements in quantitative histological markers of steatosis, inflammation, and fibrosis in GAN DIO-NASH mice. Quantitative histology for percent area of galectin3 (*A*), percent area of collagen-1a1 (*B*), percent area of α-smooth muscle actin (α-SMA; *C*), galectin3 total content (*D*), collagen 1a1 total content (*E*), α-SMA total content (*F*) n = 6–14 mice/group, $^{**}P < 0.01$, $^{***}P < 0.001$ (Dunnett's test one-factor linear model). *Bottom* panels: representative galectin-3, collagen 1a1 and α-SMA photomicrographs. DIO, diet-induced obese; GAN, Gubra Amylin NASH; NASH, nonalcoholic steatohepatitis.

GAN DIO-NASH mice, weight loss has been reported accompanied by increased food intake in response to treatment with long-acting FGF21 analogs in chow-fed mice (56, 57). Although the central and peripheral mechanisms underlying the inverse effects of long-acting FGF21 analogs on body weight and food intake are unclear, species differences in FGF21 responses should be considered when evaluating the outcomes of PF-05231023 treatment. In contrast to rodent studies, FGF21 analogs have been reported to suppress food intake in nonhuman primates (44, 47), emphasizing important species differences in the appetite regulatory effects of FGF21 analogs. Inconsistent effects of FGF21 analogs have been reported in clinical trials. While long-acting FGF21 analogs have demonstrated positive effects on insulin resistance and lipid profiles in clinical trials, the effects on body weight remain inconsistent and inconclusive (58). Previous studies in mice have reported increased thermogenesis and increased energy expenditure in response to FGF21 as potential drivers of weight loss (8, 11). It should be noted that compensatory hyperphagia is associated with FGF21-stimulated energy expenditure in mice (59–61). Brown adipose tissue (BAT) activation and increased metabolic rate as drivers of increased food intake have been described in response to cold exposure in mice (59). It should be emphasized that BAT-mediated increase in energy expenditure has limited relevance in nonhuman primates and humans (62). Although not specifically addressed in the current study, it may be speculated that PF-05231023 could promote BAT activation and hyperphagia to compensate for potentially increased energy expenditure in GAN DIO-NASH mice. Of note, low-caloric dietary intervention robustly reduces body weight and improves liver pathology but not fibrosis scores in GAN DIO-NASH mice (31). Considering that PF-05231023 also improved fibrosis scores this raises the possibility that the antifibrotic effect of PF-05231023 is, at least in part, independent of weight loss. Given the significant

AJP-Gastrointest Liver Physiol • doi:10.1152/ajpgi.00157.2022 • www.ajpgi.org

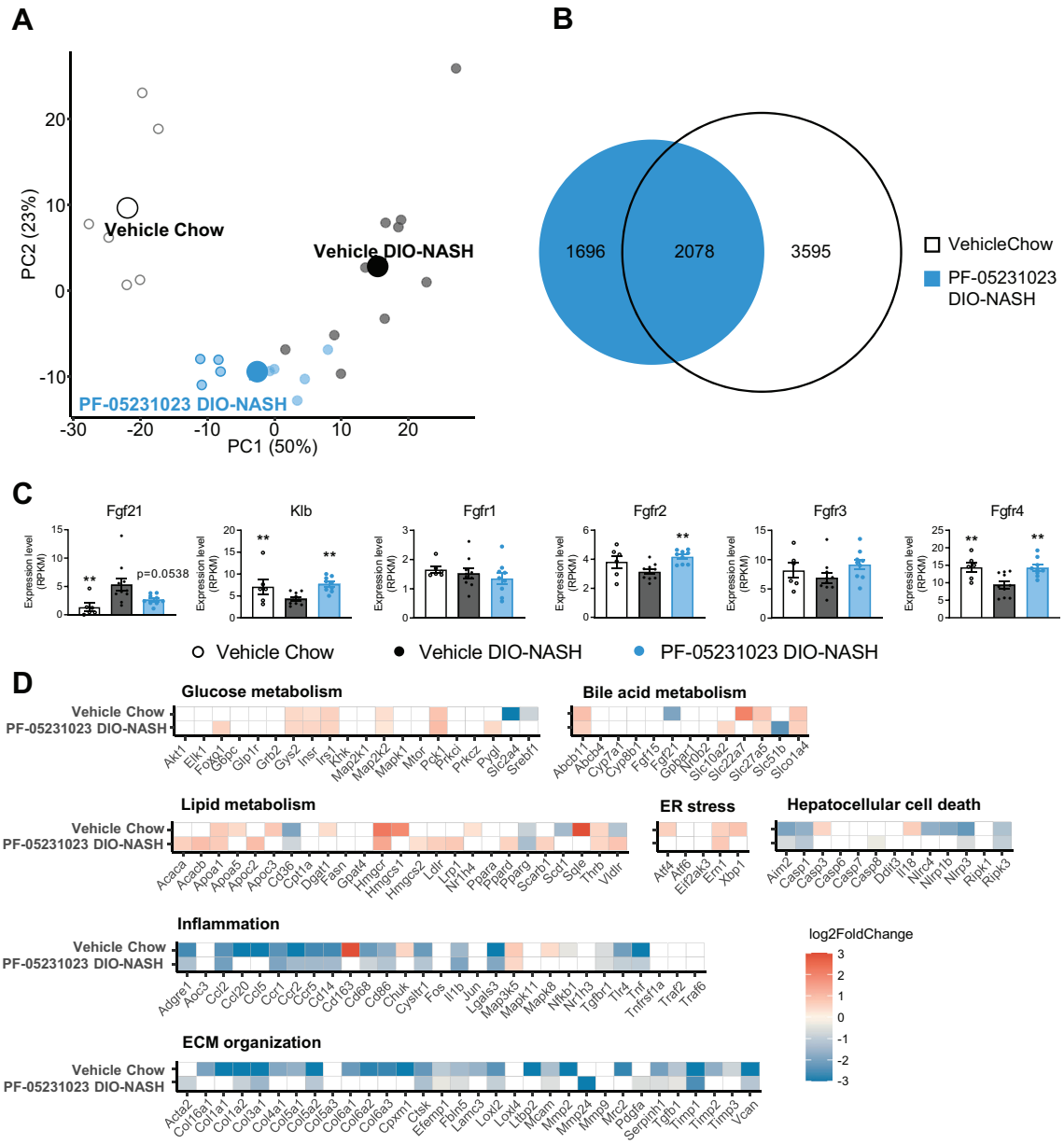

Figure 5. Changes in NASH-linked hepatic gene expression in response to PF-05231023 treatment in GAN DIO-NASH mice. *A*: principal component analysis (PCA) of samples based on top 500 most variable gene expression levels. *B*: Venn diagram depicting shared and separate differentially expressed genes in treatment groups. *C*: hepatic mRNA expression of fibroblast growth factor 21 (*Fgf21*), β-klotho (*Klb*), FGF receptor 1 (*Fgfr1*), FGF receptor 2 (*Fgfr2*), FGF receptor 3 (*Fgfr3*), and FGF receptor 4 (*Fgfr4*). Values expressed as mean of n = 6–10 mice + SE, $^{**}P < 0.01$ (false discovery rate adjusted P values, DEseq2 analysis). *D*: heatmaps depicting changes in NASH and fibrosis-associated candidate gene expression (log2-fold change compared with Vehicle DIO-NASH mice). Blue color gradients indicate significantly ($P < 0.05$) downregulated gene expression. White boxes indicate genes not significantly regulated ($P > 0.05$) compared with DIO-NASH vehicle mice (false discovery rate < 0.05). DIO, diet-induced obese; GAN, Gubra Amylin NASH; NASH, nonalcoholic steatohepatitis.

species-dependent effects of FGF21, further preclinical studies in nonrodent species must be performed to confirm anti-NASH efficacy of PF-05231023.

PF-05231023 treatment improved the liver lipid profile (reduced liver TC and liver TG) and plasma liver injury markers (ALT and AST), being in close agreement with data from clinical studies (15, 17–19) and mouse studies on FGF21 analogs (14, 25). Of note, PF-05231023 was also able to lower plasma TC in GAN DIO-NASH mice, which show hypercholesterolemia due to high dietary cholesterol levels in the GAN diet. Plasma TG in the PF-05231023 treatment group was not significantly different from the Vehicle DIO-NASH group nor Vehicle Chow. This is in contrast to previous preclinical studies in mouse models of obesity and diabetes (7, 55) and clinical trials (18, 19), describing reduced plasma TG in response to FGF21 analog treatment. The absence of hypertriglyceridemia in this model is likely attributed to suppressed hepatic triglyceride secretion as a result of the high dietary cholesterol intake, which has been shown to downregulate hepatic cholesterol ester and

lipoprotein synthesis, which impedes TG secretion from the liver (29, 63, 64).

To better understand the molecular pathways regulated by PF-05231023 treatment, we evaluated the expression of a panel of NASH-associated genes. Liver RNA sequencing analysis revealed differential expression of key genes linked to insulin signaling, glucose and lipid metabolism, inflammation, hepatocellular injury/death, ER stress, and fibrosis. These include the downregulation of prominent transcriptional targets like the potent inflammatory and fibrogenic cytokines and chemokines TGFβ1, TNF, PDGF, IL1b, and CCL2 (51, 65, 66). The improvement in fibrosis histology was paralleled by the suppression of multiple genes involved in hepatic stellate cell activation and ECM deposition, including downregulation of profibrogenic genes such as *Col1a1, Acta2, Tgfbr1,* and *Timp1*. Collectively, this suggests ongoing tissue remodeling toward lowered collagen formation resulting in lowered fibrosis.

The molecular action by which FGF21 confers beneficial metabolic effects remains a matter of debate. A study employing a liver-specific knockout of the obligate coreceptor β-klotho described intact FGF21 sensitivity thus indicating that direct FGF21 actions in the liver are dispensable for the weight loss and glycemic effects (67). This, however, is contrasted by other studies describing direct hepatic actions of FGF21 through activation of FGFR2/ERK1/2 (68) and FGFR3/KLB, which FGF21 binds to with a lower affinity (69). We find reduced liver mRNA expression of *Fgf21*, whereas receptors *FgFr2*, *Fgfr4*, and coreceptor *Klb* were upregulated upon PF-05231023 treatment, consistent with a recent study exploring native FGF21 in DIO mice (70), suggesting a demand for increased hepatic FGF signaling. Thus, although the primary receptor FGFR1 is expressed at low levels in the mouse liver, direct hepatic actions may be mediated through the stimulation of FGF receptors 2, 3, and 4. The physiological and pharmacological effects of FGF21 may also be mediated by central actions. Indeed, central infusion of FGF21 reduces body weight in rats (71). In mice, FGFR1 and KLB are coexpressed in several regions of the brain, including the hypothalamus and dorsal vagal complex (72). We therefore speculate that the hyperphagic response observed in the present study could reflect a direct central action of PF-05231023. In summary, the metabolic effects of FGF21 may therefore be mediated by a combination of direct effects in the liver, extrahepatic actions including CNS signaling and fine tuning of interorgan metabolic cross talk.

The present study confirms and extends previous reports on metabolic and hepatoprotective properties of long-acting FGF21 analogs in rodents, nonhuman primates, and patients. To our knowledge, the present study is the first to demonstrate that a long-acting FGF21 analog improves fibrosis severity in a clinical translational mouse model of NASH, supporting the development of long-acting FGF21 analogs for the treatment of NASH and other fibrotic diseases.

DATA AVAILABILITY

Data will be made available upon reasonable request.

SUPPLEMENTAL DATA

Supplemental Table S1: https://doi.org/10.6084/m9.figshare.21424488.v1.

GRANTS

This work was supported by a grant from Innovation Fund Denmark Grant 0153-00178B (to M.H.N.).

DISCLOSURES

M.H. Nielsen, N. Vrang, J. Jelsing, H.H. Hansen, M. Feigh, and D. Oró are employed by Gubra. None of the other authors has any conflicts of interest, financial or otherwise, to disclose.

AUTHOR CONTRIBUTIONS

M.H.N. conceived and designed research; M.H.N. analyzed data; M.H.N. interpreted results of experiments; M.H.N. prepared figures; M.H.N. drafted manuscript; M.H.N., M.P.G., H.H.H., M.F., and D.O. edited and revised manuscript; M.H.N., M.P.G., N.V., J.J., H.H.H., M.F., and D.O. approved final version of manuscript.

REFERENCES

1. **Younossi ZM**, **Henry L.** Epidemiology of non-alcoholic fatty liver disease and hepatocellular carcinoma. *JHEP Rep* 3: 100305, 2021. doi:10.1016/j.jhepr.2021.100305.
2. **Bedossa P.** Pathology of non-alcoholic fatty liver disease. *Liver Int* 37: 85–89, 2017. doi:10.1111/liv.13301.
3. **Smeuninx B**, **Boslem E**, **Febbraio MA.** Current and future treatments in the fight against non-alcoholic fatty liver disease. *Cancers (Basel)* 12: 1714–1722, 2020. doi:10.3390/cancers12071714.
4. **Fisher FM**, **Maratos-Flier E.** Understanding the physiology of FGF21. *Annu Rev Physiol* 78: 223–241, 2016. doi:10.1146/annurev-physiol-021115-105339.
5. **Tillman EJ**, **Rolph T.** FGF21: an emerging therapeutic target for non-alcoholic steatohepatitis and related metabolic diseases. *Front Endocrinol* 11: 1–25, 2020. doi:10.3389/fendo.2020.601290.
6. **Flippo KH**, **Potthoff MJ.** Metabolic messengers: FGF21. *Nat Metab* 3: 309–317, 2021. doi:10.1038/s42255-021-00354-2.
7. **Xu J**, **Stanislaus S**, **Chinookoswong N**, **Lau YY**, **Hager T**, **Patel J**, **Ge H**, **Weiszmann J**, **Lu SC**, **Graham M**, **Busby J**, **Hecht R**, **Li YS**, **Li Y**, **Lindberg R**, **Véniant MM.** Acute glucose-lowering and insulin-sensitizing action of FGF21 in insulin-resistant mouse models - association with liver and adipose tissue effects. *Am J Physiol Endocrinol Physiol* 297: 1105–1114, 2009. doi:10.1152/ajpendo.00348.2009.
8. **BonDurant LD**, **Ameka M**, **Naber MC**, **Markan KR**, **Idiga SO**, **Acevedo MR**, **Walsh SA**, **Ornitz DM**, **Potthoff MJ.** FGF21 regulates metabolism through adipose-dependent and -independent mechanisms. *Cell Metab* 25: 935–944.e4, 2017. doi:10.1016/j.cmet.2017.03.005.
9. **Schlein C**, **Talukdar S**, **Heine M**, **Fischer AW**, **Krott LM**, **Nilsson SK**, **Brenner MB**, **Heeren J**, **Scheja L.** FGF21 lowers plasma triglycerides by accelerating lipoprotein catabolism in white and brown adipose tissues. *Cell Metab* 23: 441–453, 2016. doi:10.1016/j.cmet.2016.01.006.
10. **Lin Z**, **Tian H**, **Lam KSL**, **Lin S**, **Hoo RCL**, **Konishi M**, **Itoh N**, **Wang Y**, **Bornstein SR**, **Xu A**, **Li X.** Adiponectin mediates the metabolic effects of FGF21 on glucose homeostasis and insulin sensitivity in mice. *Cell Metab* 17: 779–789, 2013. doi:10.1016/j.cmet.2013.04.005.
11. **Douris N**, **Stevanovic DM**, **Fisher F. M**, **Cisu TI**, **Chee MJ**, **Nguyen NL**, **Zarebidaki E**, **Adams AC**, **Kharitonenkov A**, **Flier JS**, **Bartness TJ**, **Maratos-Flier E.** Central fibroblast growth factor 21 browns white fat via sympathetic action in male mice. *Endocrinology* 156: 2470–2481, 2015. doi:10.1210/en.2014-2001.
12. **Talukdar S**, **Owen BM**, **Song P**, **Hernandez G**, **Zhang Y**, **Zhou Y**, **Scott WT**, **Paratala B**, **Turner T**, **Smith A**, **Bernardo B**, **Müller CP**, **Tang H**, **Mangelsdorf DJ**, **Goodwin B**, **Kliewer SA.** FGF21 regulates

sweet and alcohol preference. *Cell Metab* 23: 344–349, 2016. doi:10.1016/j.cmet.2015.12.008.

13. **Flippo KH**, **Trammell SAJ**, **Gillum MP**, **Aklan I**, **Perez MB**, **Yavuz Y**, **Smith NK**, **Jensen-Cody SO**, **Zhou B**, **Claflin KE**, **Beierschmitt A**, **Fink-Jensen A**, **Knop FK**, **Palmour RM**, **Grueter BA**, **Atasoy D**, **Potthoff MJ.** FGF21 suppresses alcohol consumption through an amygdalo-striatal circuit. *Cell Metab* 34: 317–328.e6, 2022. doi:10.1016/j.cmet.2021.12.024.
14. **Geng L**, **Lam KSL**, **Xu A.** The therapeutic potential of FGF21 in metabolic diseases: from bench to clinic. *Nat Rev Endocrinol* 16: 654–667, 2020. doi:10.1038/s41574-020-0386-0.
15. **Gaich G**, **Chien JY**, **Fu H**, **Glass LC**, **Deeg MA**, **Holland WL**, **Kharitonenkov A**, **Bumol T**, **Schilske HK**, **Moller DE.** The effects of LY2405319, an FGF21 Analog, in obese human subjects with type 2 diabetes. *Cell Metab* 18: 333–340, 2013. doi:10.1016/j.cmet.2013.08.005.
16. **Rader DJ**, **Maratos-Flier E**, **Nguyen A**, **Hom D**, **Ferriere M**, **Li Y**, **Kompa J**, **Martic M**, **Hinder M**, **Basson CT**, **Yowe D**, **Diener J**, **Goldfine AB**; **CLLF580X2102 Study Team.** LLF580, an FGF21 analog, reduces triglycerides and hepatic fat in obese adults with modest hypertriglyceridemia. *J Clin Endocrinol Metab* 107: e57–e70, 2022. doi:10.1210/clinem/dgab624.
17. **Harrison SA**, **Ruane PJ**, **Freilich BL**, **Neff G**, **Patil R**, **Behling CA**, **Hu C**, **Fong E**, **de Temple B**, **Tillman EJ**, **Rolph TP**, **Cheng A**, **Yale K.** Efruxifermin in non-alcoholic steatohepatitis: a randomized, double-blind, placebo-controlled, phase 2a trial. *Nat Med* 27: 1262–1271, 2021. doi:10.1038/s41591-021-01425-3.
18. **Sanyal A**, **Charles ED**, **Neuschwander-Tetri BA**, **Loomba R**, **Harrison SA**, **Abdelmalek MF**, **Lawitz EJ**, **Halegoua-DeMarzio D**, **Kundu S**, **Noviello S**, **Luo Y**, **Christian R.** Pegbelfermin (BMS-986036), a PEGylated fibroblast growth factor 21 analogue, in patients with non-alcoholic steatohepatitis: a randomised, double-blind, placebo-controlled, phase 2a trial. *Lancet* 392: 2705–2717, 2019. doi:10.1016/S0140-6736(18)31785-9.
19. **Kaufman A**, **Abuqayyas L**, **Denney WS**, **Tillman EJ**, **Rolph T.** AKR-001, an Fc-FGF21 analog, showed sustained pharmacodynamic effects on insulin sensitivity and lipid metabolism in type 2 diabetes patients. *Cell Rep Med* 1: 100057, 2020. doi:10.1016/j.xcrm.2020.100057.
20. **Mu J**, **Pinkstaff J**, **Li Z**, **Skidmore L**, **Li N**, **Myler H**, **Dallas-Yang Q**, **Putnam A-M**, **Yao J**, **Bussell S**, **Wu M**, **Norman TC**, **Rodriguez CG**, **Kimmel B**, **Metzger JM**, **Manibusan A**, **Lee D**, **Zaller DM**, **Zhang BB**, **DiMarchi RD**, **Berger JP**, **Axelrod DW.** FGF21 analogs of sustained action enabled by orthogonal biosynthesis demonstrate enhanced antidiabetic pharmacology in rodents. *Diabetes* 61: 505–512, 2012. doi:10.2337/db11-0838.
21. **Kharitonenkov A**, **Beals JM**, **Micanovic R**, **Strifler BA**, **Rathnachalam R**, **Wroblewski VJ**, **Li S**, **Koester A**, **Ford AM**, **Coskun T**, **Dunbar JD**, **Cheng CC**, **Frye CC**, **Bumol TF**, **Moller DE.** Rational design of a fibroblast growth factor 21-based clinical candidate, LY2405319. *PLoS One* 8: e58575, 2013. doi:10.1371/journal.pone.0058575.
22. **Huang J**, **Ishino T**, **Chen G**, **Rolzin P**, **Osothprarop TF**, **Retting K**, **Li L**, **Jin P**, **Matin MJ**, **Huyghe B**, **Talukdar S**, **Bradshaw CW**, **Palanki M**, **Violand BN**, **Woodnutt G**, **Lappe RW**, **Ogilvie K**, **Levin N.** Development of a novel long-acting antidiabetic FGF21 mimetic by targeted conjugation to a scaffold antibody. *J Pharmacol Exp Ther* 346: 270–280, 2013. doi:10.1124/jpet.113.204420.
23. **Liu X**, **Zhang P**, **Martin RC**, **Cui G**, **Wang G**, **Tan Y**, **Cai L**, **Lv G**, **Li Y.** Lack of fibroblast growth factor 21 accelerates metabolic liver injury characterized by steatohepatities in mice. *Am J Cancer Res* 6: 1011–1025, 2016.
24. **Zheng Q**, **Martin RC**, **Shi X**, **Pandit H**, **Yu Y**, **Liu X**, **Guo W**, **Tan M**, **Bai O**, **Meng X**, **Li Y.** Lack of FGF21 promotes NASH-HCC transition via hepatocyte-TLR4-IL-17A signaling. *Theranostics* 10: 9923–9936, 2020. doi:10.7150/thno.45988.
25. **Lee JH**, **Kang YE**, **Chang JY**, **Park KC**, **Kim HW**, **Kim JT**, **Kim HJ**, **Yi HS**, **Shong M**, **Chung HK**, **Kim KS.** An engineered FGF21 variant, LY2405319, can prevent non-alcoholic steatohepatitis by enhancing hepatic mitochondrial function *Am J Transl Res* 8: 4750–4763, 2016.
26. **Opoku YK**, **Liu Z**, **Afrifa J**, **Kumi AK**, **Liu H**, **Ghartey-Kwansah G**, **Koranteng H**, **Jiang X**, **Ren G**, **Li D.** Fibroblast growth factor-21 ameliorates hepatic encephalopathy by activating the stat3-socs3 pathway to inhibit activated hepatic stellate cells. *EXCLI J* 19: 567–581, 2020. doi:10.17179/excli2020-1287.
27. **Xu P**, **Zhang Y**, **Liu Y**, **Yuan Q**, **Song L**, **Liu M**, **Liu Z**, **Yang Y**, **Li J**, **Li D**, **Ren G.** Fibroblast growth factor 21 attenuates hepatic fibrogenesis through TGF-β/smad2/3 and NF-κB signaling pathways. *Toxicol Appl Pharmacol* 290: 43–53, 2016. doi:10.1016/j.taap.2015.11.012.
28. **Meng F**, **Khoso MH**, **Kang K**, **He Q**, **Cao Y**, **Jiang X**, **Xiao W**, **Li D.** FGF21 ameliorates hepatic fibrosis by multiple mechanisms. *Mol Biol Rep* 48: 7153–7163, 2021. doi:10.1007/s11033-021-06707-0.
29. **Boland ML**, **Oró D**, **Tølbøl KS**, **Thrane ST**, **Nielsen JC**, **Cohen TS**, **Tabor DE**, **Fernandes F**, **Tovchigrechko A**, **Veidal SS**, **Warrener P**, **Sellman BR**, **Jelsing J**, **Feigh M**, **Vrang N**, **Trevaskis JL**, **Hansen HH.** Towards a standard diet-induced and biopsy-confirmed mouse model of non-alcoholic steatohepatitis: Impact of dietary fat source. *World J Gastroenterol* 25: 4904–4920, 2019. doi:10.3748/wjg.v25.i33.4904.
30. **Hansen HH**, **Ægidius HM**, **Oró D**, **Evers SS**, **Heebøll S**, **Eriksen PL**, **Thomsen KL**, **Bengtsson A**, **Veidal SS**, **Feigh M**, **Suppli MP**, **Knop FK**, **Grønbæk H**, **Miranda D**, **Trevaskis JL**, **Vrang N**, **Jelsing J**, **Rigbolt KTG.** Human translatability of the GAN diet-induced obese mouse model of non-alcoholic steatohepatitis. *BMC Gastroenterol* 20: 1–12, 2020. doi:10.1186/s12876-020-01356-2.
31. **Møllerhøj MB**, **Veidal SS**, **Thrane KT**, **Oró D**, **Overgaard A**, **Salinas CG**, **Madsen MR**, **Pfisterer L**, **Vyberg M**, **Simon E**, **Broermann A**, **Vrang N**, **Jelsing J**, **Feigh M**, **Hansen HH.** Hepatoprotective effects of semaglutide, lanifibranor and dietary intervention in the GAN diet-induced obese and biopsy-confirmed mouse model of NASH. *Clin Transl Sci* 1167–1186, 2022. doi:10.1111/cts.13235.
32. **O'Farrell M**, **Duke G**, **Crowley R**, **Buckley D**, **Martins EB**, **Bhattacharya D**, **Friedman SL**, **Kemble G.** FASN inhibition targets multiple drivers of NASH by reducing steatosis, inflammation and fibrosis in preclinical models. *Sci Rep* 12: 15661, 2022. doi:10.1038/s41598-022-19459-z.
33. **Zhou B**, **Luo Y**, **Ji N**, **Hu C**, **Lu Y.** Orosomucoid 2 maintains hepatic lipid homeostasis through suppression of de novo lipogenesis. *Nat Metab* 4: 1185–1201, 2022. doi:10.1038/s42255-022-00627-4.
34. **Gao R**, **Wang J**, **He X**, **Wang T**, **Zhou L**, **Ren Z**, **Yang J**, **Xiang X**, **Wen S**, **Yu Z**, **Ai H**, **Wang Y**, **Liang H**, **Li S**, **Lu Y**, **Zhu Y**, **Shi G**, **Chen Y.** Comprehensive analysis of endoplasmic reticulum-related and secretome gene expression profiles in the progression of non-alcoholic fatty liver disease. *Front Endocrinol (Lausanne)* 13: 967016, 2022. doi:10.3389/fendo.2022.967016.
35. **Steffen J**, **Ngo J**, **Wang S-P**, **Williams K**, **Kramer HF**, **Ho G**, **Rodriguez C**, **Yekkala K**, **Amuzie C**, **Bialecki R**, **Norquay L**, **Nawrocki AR**, **Erion M**, **Pocai A**, **Shirihai OS**, **Liesa M.** The mitochondrial fission protein Drp1 in liver is required to mitigate NASH and prevents the activation of the mitochondrial ISR. *Mol Metab* 64: 101566, 2022. doi:10.1016/j.molmet.2022.101566.
36. **Kayed A**, **Melander SA**, **Khan S**, **Andreassen KV**, **Karsdal MA**, **Henriksen K.** The effects of dual GLP-1/Glucagon receptor agonists with different receptor selectivity in mouse models of obesity and NASH. *J Pharmacol Exp Ther* 384: 406–416, 2022. doi:10.1124/jpet.122.001440.
37. **Guo L**, **Zhang P**, **Chen Z**, **Xia H**, **Li S**, **Zhang Y**, **Kobberup S**, **Zou W**, **Lin JD.** Hepatic neuregulin 4 signaling defines an endocrine checkpoint for steatosis-to-NASH progression. *J Clin Invest* 127: 4449–4461, 2017. doi:10.1172/JCI96324.
38. **Liu B**, **Xiang L**, **Ji J**, **Liu W**, **Chen Y**, **Xia M**, **Liu Y**, **Liu W**, **Zhu P**, **Jin Y**, **Han Y**, **Lu J**, **Li X**, **Zheng M**, **Lu Y.** Sparcl1 promotes nonalcoholic steatohepatitis progression in mice through upregulation of CCL2. *J Clin Invest* 131: e144801, 2021. doi:10.1172/JCI144801.
39. **Clapper JR**, **Hendricks MD**, **Gu G**, **Wittmer C**, **Dolman CS**, **Herich J**, **Athanacio J**, **Villescaz C**, **Ghosh SS**, **Heilig JS**, **Lowe C**, **Roth JD.** Diet-induced mouse model of fatty liver disease and nonalcoholic steatohepatitis reflecting clinical disease progression and methods of assessment. *Am J Physiol Gastrointest Liver Physiol* 305: G483–G495, 2013. doi:10.1152/ajpgi.00079.2013.
40. **Kristiansen MNB**, **Veidal SS**, **Rigbolt KTG**, **Tølbøl KS**, **Roth JD**, **Jelsing J**, **Vrang N**, **Feigh M.** Obese diet-induced mouse models of nonalcoholic steatohepatitis-tracking disease by liver biopsy. *World J Hepatol* 8: 673–684, 2016. doi:10.4254/wjh.v8.i16.673.
41. **Tølbøl KS**, **Kristiansen MN**, **Hansen HH**, **Veidal SS**, **Rigbolt KT**, **Gillum MP**, **Jelsing J**, **Vrang N**, **Feigh M.** Metabolic and hepatic effects of liraglutide, obeticholic acid and elafibranor in diet-induced obese mouse models of biopsy-confirmed nonalcoholic steatohepatitis. *World J Gastroenterol* 24: 179–194, 2018. doi:10.3748/wjg.v24.i2.179.

42. **Trevaskis JL**, **Griffin PS**, **Wittmer C**, **Neuschwander-Tetri BA**, **Brunt EM**, **Dolman CS**, **Erickson MR**, **Napora J**, **Parkes DG**, **Roth JD.** Glucagon-like peptide-1 receptor agonism improves metabolic, biochemical, and histopathological indices of nonalcoholic steatohepatitis in mice. *Am J Physiol Gastrointest Liver Physiol* 302: 762–772, 2012. doi:10.1152/ajpgi.00476.2011.
43. **Gallage S**, **Avila JEB**, **Ramadori P**, **Focaccia E**, **Rahbari M**, **Ali A**, **Malek NP**, **Anstee QM**, **Heikenwalder M.** A researcher ' s guide to preclinical mouse NASH models. *Nat Metab* 4: 1632–1649, 2022. doi:10.1038/s42255-022-00700-y.
44. **Talukdar S**, **Zhou Y**, **Li D**, **Rossulek M**, **Dong J**, **Somayaji V**, **Weng Y**, **Clark R**, **Lanba A**, **Owen BM**, **Brenner MB**, **Trimmer JK**, **Gropp KE**, **Chabot JR**, **Erion DM**, **Rolph TP**, **Goodwin B**, **Calle RA.** A long-acting FGF21 molecule, PF-05231023, decreases body weight and improves lipid profile in non-human primates and type 2 diabetic subjects. *Cell Metab* 23: 427–440, 2016. doi:10.1016/j.cmet.2016.02.001.
45. **Kim AM**, **Somayaji VR**, **Dong JQ**, **Rolph TP**, **Weng Y**, **Chabot JR**, **Gropp KE**, **Talukdar S**, **Calle RA.** Once-weekly administration of a long-acting fibroblast growth factor 21 analogue modulates lipids, bone turnover markers, blood pressure and body weight differently in obese people with hypertriglyceridaemia and in non-human primates. *Diabetes Obes Metab* 19: 1762–1772, 2017. doi:10.1111/dom.13023.
46. **Weng Y**, **Chabot JR**, **Bernardo B**, **Yan Q**, **Zhu Y**, **Brenner MB**, **Vage C**, **Logan A**, **Calle R**, **Talukdar S.** Pharmacokinetics (PK), pharmacodynamics (PD) and integrated PK/PD modeling of a novel long acting FGF21 clinical candidate PF-05231023 in diet-induced obese and leptin-deficient obese mice. *PLoS One* 10: e0119104, 2015. doi:10.1371/journal.pone.0119104.
47. **Thompson WC**, **Zhou Y**, **Talukdar S**, **Musante CJ.** PF-05231023, a long-acting FGF21 analogue, decreases body weight by reduction of food intake in non-human primates. *J Pharmacokinet Pharmacodyn* 43: 411–425, 2016. doi:10.1007/s10928-016-9481-1.
48. **Kleiner DE**, **Brunt EM**, **Van Natta M**, **Behling C**, **Contos MJ**, **Cummings OW**, **Ferrell LD**, **Liu Y-C**, **Torbenson MS**, **Unalp-Arida A**, **Yeh M**, **McCullough AJ**, **Sanyal AJ**; **Nonalcoholic Steatohepatitis Clinical Research Network.** Design and validation of a histological scoring system for nonalcoholic fatty liver disease. *Hepatology* 41: 1313–1321, 2005. doi:10.1002/hep.20701.
49. **Baandrup Kristiansen MN**, **Veidal SS**, **Christoffersen C**, **Feigh M**, **Vrang N**, **Roth JD**, **Erickson M**, **Adorini L**, **Jelsing J.** Validity of biopsy-based drug effects in a diet-induced obese mouse model of biopsy-confirmed NASH. *BMC Gastroenterol* 19: 228, 2019. doi:10.1186/s12876-019-1149-z.
50. **Fabregat A**, **Jupe S**, **Matthews L**, **Sidiropoulos K**, **Gillespie M**, **Garapati P**, **Haw R**, **Jassal B**, **Korninger F**, **May B**, **Milacic M**, **Roca CD**, **Rothfels K**, **Sevilla C**, **Shamovsky V**, **Shorser S**, **Varusai T**, **Viteri G**, **Weiser J**, **Wu G**, **Stein L**, **Hermjakob H**, **D'Eustachio P.** The reactome pathway knowledgebase. *Nucleic Acids Res* 46: D649–D655, 2018. doi:10.1093/nar/gkx1132.
51. **Tsuchida T**, **Friedman SL.** Mechanisms of hepatic stellate cell activation. *Nat Rev Gastroenterol Hepatol* 14: 397–411, 2017. doi:10.1038/nrgastro.2017.38.
52. **Younossi ZM**, **Stepanova M**, **Lawitz E**, **Charlton M**, **Loomba R**, **Myers RP**, **Subramanian M**, **McHutchison JG**, **Goodman Z.** Improvement of hepatic fibrosis and patient-reported outcomes in non-alcoholic steatohepatitis treated with selonsertib. *Liver Int* 38: 1849–1859, 2018. doi:10.1111/liv.13706.
53. **Angulo P**, **Kleiner DE**, **Dam-Larsen S**, **Adams LA**, **Bjornsson ES**, **Charatcharoenwitthaya P**, **Mills PR**, **Keach JC**, **Lafferty HD**, **Stahler A**, **Haflidadottir S**, **Bendtsen F.** Liver fibrosis, but no other histologic features, is associated with long-term outcomes of patients with nonalcoholic fatty liver disease. *Gastroenterology* 149: 389–397.e10, 2015. doi:10.1053/j.gastro.2015.04.043.
54. **Xu J**, **Lloyd DJ**, **Hale C**, **Stanislaus S**, **Chen M**, **Sivits G**, **Vonderfecht S**, **Hecht R**, **Li YS**, **Lindberg RA**, **Chen JL**, **Jung DY**, **Zhang Z**, **Ko HJ**, **Kim JK**, **Véniant MM.** Fibroblast growth factor 21 reverses hepatic steatosis, increases energy expenditure, and improves insulin sensitivity in diet-induced obese mice. *Diabetes* 58: 250–259, 2009. doi:10.2337/db08-0392.
55. **Coskun T**, **Bina HA**, **Schneider MA**, **Dunbar JD**, **Hu CC**, **Chen Y**, **Moller DE**, **Kharitonenkov A.** Fibroblast growth factor 21 corrects obesity in mice. *Endocrinology* 149: 6018–6027, 2008. doi:10.1210/en.2008-0816.
56. **Claflin KE**, **Sullivan AI**, **Naber MC**, **Flippo KH**, **Morgan DA**, **Neff TJ**, **Jensen-Cody SO**, **Zhu Z**, **Zingman LV**, **Rahmouni K**, **Potthoff MJ.** Pharmacological FGF21 signals to glutamatergic neurons to enhance leptin action and lower body weight during obesity. *Mol Metab* 64: 101564, 2022. doi:10.1016/j.molmet.2022.101564.
57. **Véniant MM**, **Sivits G**, **Helmering J**, **Komorowski R**, **Lee J**, **Fan W**, **Moyer C**, **Lloyd DJ.** Pharmacologic effects of FGF21 are independent of the "Browning" of white adipose tissue. *Cell Metab* 21: 731–738, 2015. doi:10.1016/j.cmet.2015.04.019.
58. **Shao W**, **Jin T.** Hepatic hormone FGF21 and its analogues in clinical trials. *Chronic Dis Transl Med* 8: 19–25, 2022. doi:10.1016/j.cdtm.2021.08.005.
59. **Ravussin Y**, **Xiao C**, **Gavrilova O**, **Reitman ML.** Effect of intermittent cold exposure on brown fat activation, obesity, and energy homeostasis in mice. *PLoS One* 9: e85876, 2014. doi:10.1371/journal.pone.0085876.
60. **Owen BM**, **Ding X**, **Morgan DA**, **Coate KC**, **Bookout AL**, **Rahmouni K**, **Kliewer SA**, **Mangelsdorf DJ.** FGF21 acts centrally to induce sympathetic nerve activity, energy expenditure, and weight loss. *Cell Metab* 20: 670–677, 2014. doi:10.1016/j.cmet.2014.07.012.
61. **Hill CM**, **Laeger T**, **Dehner M**, **Albarado DC**, **Clarke B**, **Wanders D**, **Burke SJ**, **Collier JJ**, **Qualls-Creekmore E**, **Solon-Biet SM**, **Simpson SJ**, **Berthoud HR**, **Münzberg H**, **Morrison CD.** FGF21 signals protein status to the brain and adaptively regulates food choice and metabolism. *Cell Rep* 27: 2934–2947.e3, 2019. doi:10.1016/j.celrep.2019.05.022.
62. **Carpentier AC**, **Blondin DP**, **Virtanen KA**, **Richard D**, **Haman F**, **Turcotte ÉE.** Brown adipose tissue energy metabolism in humans. *Front Endocrinol (Lausanne)* 9: 447, 2018. doi:10.3389/fendo.2018.00447.
63. **Ma K**, **Malhotra P**, **Soni V**, **Hedroug O**, **Annaba F**, **Dudeja A**, **Shen L**, **Turner JR**, **Khramtsova EA**, **Saksena S**, **Dudeja PK**, **Gill RK**, **Alrefai WA.** Overactivation of intestinal SREBP2 in mice increases serum cholesterol. *PLoS One* 9: e84221, 2014. doi:10.1371/journal.pone.0084221.
64. **Henkel J**, **Coleman CD**, **Schraplau A**, **Jöhrens K**, **Weber D**, **Castro JP**, **Hugo M**, **Schulz TJ**, **Krämer S**, **Schürmann A**, **Püschel GP.** Induction of steatohepatitis (NASH) with insulin resistance in wild-type B6 mice by a western-type diet containing soybean oil and cholesterol. *Mol Med* 23: 70–82, 2017. doi:10.2119/molmed.2016.00203.
65. **Wong L**, **Yamasaki G**, **Johnson RJ**, **Friedman SL.** Induction of β-platelet-derived growth factor receptor in rat hepatic lipocytes during cellular activation in vivo and in culture. *J Clin Invest* 94: 1563–1569, 1994. doi:10.1172/JCI117497.
66. **Hellerbrand C**, **Stefanovic B**, **Giordano F**, **Burchardt ER**, **Brenner DA.** The role of TGFβ1 in initiating hepatic stellate cell activation in vivo. *J Hepatol* 30: 77–87, 1999. doi:10.1016/s0168-8278(99)80010-5.
67. **Lan T**, **Morgan DA**, **Rahmouni K**, **Sonoda J**, **Fu X**, **Burgess SC**, **Holland WL**, **Kliewer SA**, **Mangelsdorf DJ.** FGF19, FGF21, and an FGFR1/β-Klotho-activating antibody act on the nervous system to regulate body weight and glycemia. *Cell Metab* 26: 709–718.e3, 2017. doi:10.1016/j.cmet.2017.09.005.
68. **Fisher FM**, **Estall JL**, **Adams AC**, **Antonellis PJ**, **Bina HA**, **Flier JS**, **Kharitonenkov A**, **Spiegelman BM**, **Maratos-Flier E.** Integrated regulation of hepatic metabolism by fibroblast growth factor 21 (FGF21) in vivo. *Endocrinology* 152: 2996–3004, 2011. doi:10.1210/en.2011-0281.
69. **Ogawa Y**, **Kurosu H**, **Yamamoto M**, **Nandi A**, **Rosenblatt KP**, **Goetz R**, **Eliseenkova AV**, **Mohammadi M**, **Kuro-o M.** βKlotho is required for metabolic activity of fibroblast growth factor 21. *Proc Natl Acad Sci USA* 104: 7432–7437, 2007. doi:10.1073/pnas.0701600104.
70. **Keinicke H**, **Sun G**, **Mentzel CMJ**, **Fredholm M**, **John LM**, **Andersen B**, **Raun K**, **Kjaergaard M.** Fgf21 regulates hepatic metabolic pathways to improve steatosis and inflammation. *Endocr Connect* 9: 755–768, 2020. doi:10.1530/EC-20-0152.
71. **Yilmaz U**, **Tekin S**, **Demir M**, **Cigremis Y**, **Sandal S.** Effects of central FGF21 infusion on the hypothalamus–pituitary–thyroid axis and energy metabolism in rats. *J Physiol Sci* 68: 781–788, 2018. doi:10.1007/s12576-018-0595-7.
72. **Bookout AL**, **de Groot MH**, **Owen BM**, **Lee S**, **Gautron L**, **Lawrence HL**, **Ding X**, **Elmquist JK**, **Takahashi JS**, **Mangelsdorf DJ**, **Kliewer SA.** FGF21 regulates metabolism and circadian behavior by acting on the nervous system. *Nat Med* 19: 1147–1152, 2013. doi:10.1038/nm.3249.